Hindawi
Discrete Dynamics in Nature and Society
Volume 2023, Article ID 5633737, 11 pages
https://doi.org/10.1155/2023/5633737

Research Article

State Feedback H∞ Control for Trajectory Tracking of an Unmanned Surface Vehicle

Shufang Zhuo,[1] **Yonghui He**,[1] **and Yanwei Huang**[2]

[1]*College of Digital Technology, Fujian Polytechnic of Information Technology, Fuzhou 350003, China*
[2]*Department of Automation, Fuzhou University, Fuzhou 350116, China*

Correspondence should be addressed to Shufang Zhuo; zhuo_sf@163.com

Received 30 May 2023; Revised 10 September 2023; Accepted 26 September 2023; Published 18 October 2023

Academic Editor: Xiaoquan Wang

Aiming at the sway velocity and uncertainties such as wind, wave, and current, a state feedback H∞ control method is proposed to improve the dynamic and steady-state performance with line of sight (LOS) law for trajectory tracking of an unmanned surface vehicle (USV). First, a novel LOS is proposed for trajectory tracking with the position error to obtain the references of surge velocity and heading angle. Second, the LPV model is established with varying parameters of the sway velocity for the USV. Third, the closed-loop system for the LPV model is established by the state feedback H∞ control method to design the controller. Since the coupling term of system coefficients in the Lyapunov stability condition is difficult to solve directly, a novel variable is introduced to decouple the stability condition, which can be solved with MATLAB LMI tools for the controller parameters. Finally, the simulation result shows that the proposed method has super performance on the dynamic and steady-state indices.

1. Introduction

The trajectory tracking is a key technology to autonomously navigate to execute various tasks for an unmanned surface vehicle (USV) [1]. Since there are many disturbances in river or ocean, such as wind, wave, and current, an accurate mathematical model is too difficult to be established for the USV to obtain an excellent performance of trajectory tracking. In order to improve the performance of trajectory tracking, the novel control technologies are always explored and presented for the USV.

The trajectory tracking technology for the USV is classified into two strategies of the direct and indirect method. The indirect method includes the guidance law and the controller of the heading angle and velocity. For the guidance law, the line of sight (LOS) guidance law is a useful method in the path following and trajectory tracking fields [2]. A modified LOS is proposed for an adaptive sliding mode path following of the USV to suppress unknown constant current and other external disturbances [3]. An improved integral LOS with time-varying look-ahead distance is proposed for a path-following control system for USV [4]. The look-ahead distance is a function of USV's cruising speed and cross tracking errors. In order to eliminate the tracking errors, the dynamic equation of the tracking error is established with the time-varying current in Serret–Frenet coordinate system, and LOS is modified by the adaptive law of three variables to replace the unmeasurable current and side slip angle [5]. These modified LOS laws focus on the heading angle to reduce the following errors with the disturbance for path following. For trajectory tracking, LOS should simultaneously produce the surge velocity reference and the heading angle reference [6]. Here, a novel LOS will be presented to design the control variable references of surge velocity and heading angle for trajectory tracking to converge to the desired trajectory. To improve the system performance, many research achievements on trajectory tracking technology have been obtained in the past decade [7]. Many advanced control technologies are proposed for the trajectory tracking of USV, for example, the PID algorithm [8], sliding mode control (SMC) [1, 9, 10], backstepping method [11], andneural network [12]. Since there are many disturbances in water way, such as wind and waves, a robust control technology is always a useful method

to achieve an excellent trajectory tracking performance in complex environments. A μ-synthesis robust controller is designed to suppress the uncertainties of the Nomoto model of USV and the disturbances caused by waves [13]. Considering the influence of varying surge velocity on heading control, a state feedback H∞ heading control is proposed for the LPV model with surge velocity [14]. A linear parameter varying (LPV) model was presented with varied velocity parameters to adjust the course under different velocity conditions [15]. A robust H∞ heading control method based on convex hull is proposed to effectively suppress the adverse effect of system uncertainty [16]. A state feedback (SF) H∞ robust controller is proposed for the LPV model with variable mass parameters without considerations of USV sway velocity [17]. Due to the influence of wind and wave on the current surface, the roll speed of the USV almost exists in the process of steering, which results in an increment of the sway velocity [18]. So, it is very important for the design on SF H∞ controller with the consideration of the sway velocity to improve the system performance of trajectory tracking.

Here, the SF H∞ method is proposed for trajectory tracking of USV with considerations of sway velocities to suppress the uncertainties and disturbances, including the design on the LOS guidance law and the controller. First, the position error model of USV's motion is established for trajectory tracking. Second, a novel LOS with the position errors is proposed to produce the heading angle reference and the surge velocity reference for trajectory tracking to guarantee that the USV converge to the desired trajectory quickly. Third, the LPV model is established with different sway velocities for the USV dynamic model, and the SF H∞ method is used to design the closed loop system of the LPV model with the Lyapunov function. Since the Lyapunov function has the coupling term of system parameter matrix parameters, it is decoupled with the novel variable to obtain the stability condition. Moreover, the stability condition is a linear matrix inequality to be solved by the MATLAB LMI toolbox for the controller parameters. Finally, the proposed SF control method for trajectory tracking is verified effective to suppress the influence of sway velocities and has a super dynamic and stable state system performance through the simulation comparisons.

This paper is organized as follows. In Section 2, the USV motion error model is established. In Section 3, an error correction is introduced to design the LOS guidance law. In Section 4, SF controller is designed to obtain the lateral torque control law and longitudinal thrust control law. Finally, the simulation result is discussed in Section 5.

2. Position Error Model of USV Motion

2.1. Kinematics Model. Since the earth is supposed as a plane, Figure 1 shows the motion diagram of USV. (x, y) is the center position of USV's mass in the earth coordinate, (x_d, y_d) is the position to be tracked, ψ_d is the desired heading angle, ψ is the heading angle, u, v, and r are the surge velocity, sway velocity, and yaw velocity of USV, respectively.

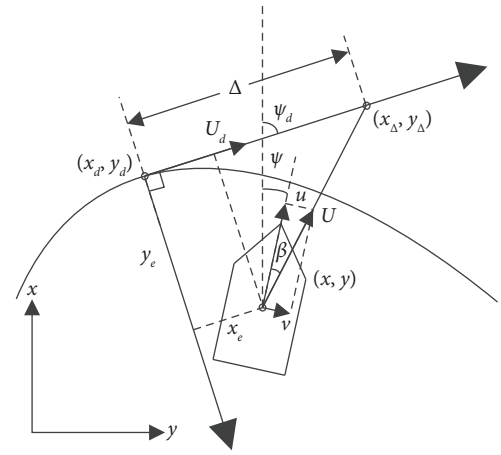

Figure 1: Trajectory tracking diagram.

The kinematics mathematical motion model is as follows [19]:

$$\begin{cases} \dot{x} = u\cos\psi - v\sin\psi, \\ \dot{y} = u\sin\psi + v\cos\psi, \\ \dot{\psi} = r. \end{cases} \tag{1}$$

Usually, USV is assumed as symmetry both from front to rear and from left to right, and the mass center is located in the hull center. With the system parameter uncertainties, the dynamic model is as follows [19]:

$$\begin{cases} m_{11}\dot{u} - m_{22}\mathrm{vr} + d_{11}u = \tau_u + \tau_{\mathrm{uw}}, \\ m_{22}\dot{v} + m_{11}\mathrm{ur} + d_{22}v = \tau_{\mathrm{vw}}, \\ m_{33}\dot{r} + (m_{22} - m_{11})uv + d_{33}r = \tau_r + \tau_{\mathrm{rw}}, \end{cases} \tag{2}$$

where d_{11}, d_{22}, d_{33}, m_{11}, m_{22}, and m_{33} are the hydrodynamic damping coefficients and the inertial parameters including the additional mass. τ_u and τ_r are the longitudinal thrust and lateral steering torque, respectively; τ_{uw}, τ_{vw}, and τ_{rw} are the interference forces and torques of the USV generated by external wind, waves, and currents, respectively.

2.2. Position Error Model of Trajectory Tracking. In Figure 1, along the tangent and centripetal direction through the point (x_d, y_d), the position tracking errors of tangent error x_e and centripetal error y_e are defined as follows:

$$\begin{bmatrix} x_e \\ y_e \end{bmatrix} = \begin{bmatrix} \cos\psi_d & \sin\psi_d \\ -\sin\psi_d & \cos\psi_d \end{bmatrix} \begin{bmatrix} x - x_d \\ y - y_d \end{bmatrix}, \tag{3}$$

where $\psi_d \in [-\pi, \pi]$, and ψ_d is as follows:

$$\psi_d = \mathrm{atan}\,2(\dot{y}_d, \dot{x}_d), \tag{4}$$

where atan2 is the arctangent function.

In Figure 1, the speed U_d on desired trajectory is as follows [6]:

$$U_d = \dot{x}_d\cos\psi_d + \dot{y}_d\sin\psi_d = \sqrt{\dot{x}_d^2 + \dot{y}_d^2}. \tag{5}$$

With equations (1) and (5), the derivative of equation (3) is as follows:

$$\begin{aligned}\dot{x}_e &= \dot{x}\cos\psi_d + \dot{y}\sin\psi_d - \left(\dot{x}_d\cos\psi_d + \dot{y}_d\sin\psi_d\right) + \dot{\psi}_d\left(-(x-x_d)\sin\psi_d + (y-y_d)\cos\psi_d\right)\\ &= u\cos\psi\cos\psi_d + u\sin\psi\sin\psi_d - \left(v\sin\psi\cos\psi_d - v\cos\psi\sin\psi_d\right) - U_d + \dot{\psi}_d y_e\\ &= U\cos\beta\cos\left(\psi-\psi_d\right) - U\sin\beta\sin\left(\psi-\psi_d\right) + \dot{\psi}_d y_e - U_d\\ &= U\cos\left(\psi-\psi_d+\beta\right) + \dot{\psi}_d y_e - U_d,\end{aligned} \tag{6}$$

$$\begin{aligned}\dot{y}_e &= \dot{y}\cos\psi_d - \dot{x}\sin\psi_d + \left(\dot{x}_d\sin\psi_d - \dot{y}_d\cos\psi_d\right) - \dot{\psi}_d\left((x-x_d)\cos\psi_d + (y-y_d)\sin\psi_d\right)\\ &= u\sin\psi\cos\psi_d - u\cos\psi\sin\psi_d + v\cos\psi\cos\psi_d + v\sin\psi\sin\psi_d) - U_d - \dot{\psi}_d x_e\\ &= U\cos\beta\sin\left(\psi-\psi_d\right) + U\sin\beta\cos\left(\psi-\psi_d\right) - \dot{\psi}_d x_e\\ &= U\sin\left(\psi-\psi_d+\beta\right) - \dot{\psi}_d x_e,\end{aligned} \tag{7}$$

where $U = \sqrt{u^2+v^2}$ is the combined speed of USV, and $\beta = \text{atan2}(v,u) \in [-\pi,\pi]$ is the sideslip angle, produced by the sway velocity v. Equations (6) and (7) are the dynamic models with position error for USV trajectory tracking.

3. LOS with Position Errors for Trajectory Tracking

For trajectory tracking, LOS should produce both the reference of heading angle and the reference of surge velocity.

3.1. LOS for the Heading Angle. The Lyapunov function V is defined as follows:

$$V = \frac{1}{2}\left(x_e^2 + y_e^2\right). \tag{8}$$

The derivative of equation (8) is as follows:

$$\begin{aligned}\dot{V} &= x_e\dot{x}_e + y_e\dot{y}_e\\ &= x_e\left(U\cos\left(\psi-\psi_d+\beta\right) + \dot{\psi}_d y_e - U_d\right) + y_e\left(U\sin\left(\psi-\psi_d+\beta\right) - \dot{\psi}_d x_e\right)\\ &= x_e U\cos\left(\psi-\psi_d+\beta\right) + x_e U_d + y_e U\sin\left(\psi-\psi_d+\beta\right).\end{aligned} \tag{9}$$

In Figure 1, (x_Δ, y_Δ) is the position in the tangential direction and Δ is the distance between (x_d, y_d) and (x_Δ, y_Δ). In order to regulate the USV's heading angle to (x_Δ, y_Δ), LOS for the heading angle is designed as follows:

$$\psi_r = \psi_d - \beta - \arctan\left(\frac{y_e}{\Delta - x_e}\right), \tag{10}$$

where ψ_r is the reference heading angle by LOS.

3.2. LOS for Surge Velocity. If the control system of the heading angle has an excellent performance, which is supposed as $\psi = \psi_r$, equation (9) is as follows:

$$\begin{aligned}\dot{V} &= x_e U\cos\left(-\arctan\left(\frac{y_e}{\Delta-x_e}\right)\right) + x_e U_d + y_e U\sin\left(-\arctan\left(\frac{y_e}{\Delta-x_e}\right)\right)\\ &= x_e\left(\frac{\Delta-x_e}{\sqrt{y_e^2+(\Delta-x_e)^2}}U - U_d\right) - \frac{y_e^2}{\sqrt{y_e^2+(\Delta-x_e)^2}}U.\end{aligned} \tag{11}$$

The reference speed U_r of USV is designed as follows:

$$U_r = \frac{(U_d - kx_e)\sqrt{y_e^2 + (\Delta - x_e)^2}}{\Delta - x_e}, \tag{12}$$

where $k > 0$.

If $U = U_r$, equation (11) is as follows:

$$\dot{V} = -\frac{U y_e^2}{\sqrt{y_e^2 + (\Delta - x_e)^2}} - \mathrm{k}x_e^2 < 0. \tag{13}$$

Since U and $k > 0$, $\dot{V} < 0$ always holds for any x_e and y_e. In order to assure x_e and y_e converge to zero to track the desired trajectory for USV, the longitudinal thrust control law and the lateral torque control law should be designed for U and ψ to converge to U_r and ψ_r.

Since USV is an underactuated system without lateral driving force, the lateral torque is usually small to prevent accidents. If the sway velocity is assumed to be small, the reference surge velocity u_r is equal to U_r in equation (12), i.e.,

$$u_r \approx U_r, \tag{14}$$

where u_r is the surge velocity by LOS.

When the actual heading angle ψ and the surge velocity u of USV can track ψ_r and u_r, x_e and y_e can converge to zero, which means the USV can track the desired trajectory. So, it is important to design longitudinal thrust controller and the lateral torque controller to ensure U and ψ converge to U_r and ψ_r quickly.

4. SF Control for the LPV System

4.1. LPV System with Sway Velocity. The heading angle error ψ_e is defined as follows:

$$\psi_e = \psi_r - \psi, \tag{15}$$

where ψ_r is assumed to be constant in a sampling cycle, the derivative of equation (15) is as follows:

$$\dot{\psi}_e = -\dot{\psi} = -r. \tag{16}$$

Surge velocity error u_e is defined as follows:

$$u_e = u_r - u, \tag{17}$$

where u_r is also assumed to be constant in a sampling cycle. With equation (17), equation (2) is as follows:

$$\begin{cases} -\dot{u_e} = \dfrac{1}{m_{11}}\left[-d_{11}(u_r - u_e) + m_{22}\mathrm{vr} + \tau_u + \tau_{\mathrm{uw}}\right], \\ \dot{r} = \dfrac{1}{m_{33}}\left[(m_{11} - m_{22})(u_r - u_e)v - d_{33}r + \tau_r + \tau_{\mathrm{rw}}\right]. \end{cases} \tag{18}$$

The novel variables are designed as follows:

$$\begin{aligned} \widetilde{\tau}_u &= d_{11}u_r - \tau_u, \\ \widetilde{\tau}_r &= (m_{11} - m_{22})\mathrm{vu}_r + \tau_r. \end{aligned} \tag{19}$$

The state variable is $\xi = [u_e,\ r,\ \psi_e]^T$, and the system measurement output y is the heading angle error ψ_e. The system state equations with equation (16) and (18) are as follows:

$$\begin{cases} \dot{\xi} = A(v)\xi + B_1 w + B_2 \tau, \\ y = C_2 \xi, \\ z = C_1 \xi, \end{cases} \tag{20}$$

where z is the modulated output and $A(v)$ is the system coefficient matrix with the relation of the sway velocity v, i.e.,

$$\begin{aligned} A(v) &= \begin{bmatrix} -\dfrac{d_{11}}{m_{11}} & -\dfrac{m_{22}v}{m_{11}} & 0 \\ \dfrac{(m_{22} - m_{11})v}{m_{33}} & -\dfrac{d_{33}}{m_{33}} & 0 \\ 0 & -1 & 0 \end{bmatrix}, \\ B_1 &= \begin{bmatrix} \dfrac{1}{m_{11}} & 0 \\ 0 & \dfrac{1}{m_{33}} \\ 0 & 0 \end{bmatrix}, \\ B_2 &= \begin{bmatrix} \dfrac{-1}{m_{11}} & 0 \\ 0 & \dfrac{1}{m_{33}} \\ 0 & 0 \end{bmatrix}, \\ C_1 &= \begin{bmatrix} 1 & 0 & 0 \\ 0 & 0 & 1 \end{bmatrix}, \\ C_2 &= \begin{bmatrix} 0 & 0 & 1 \end{bmatrix}, \\ \tau &= \begin{bmatrix} \widetilde{\tau}_u & \widetilde{\tau}_r \end{bmatrix}^T, \\ w &= \begin{bmatrix} \tau_{uw} & \tau_{rw} \end{bmatrix}^T, \end{aligned} \tag{21}$$

where B_1, B_2, C_1, C_2 are the system constant coefficients, τ is the torque control variable, and w is the disturbance vector. Equation (20) is the LPV system with sway velocity v and the uncertainty w for USV.

4.2. SF H∞ Controller Design. The SF H∞ control method is proposed for the LPV system of equation (20). The control variable τ is as follows:

$$\tau = K\xi, \tag{22}$$

where K is the controller parameter to be solved. With the control variable τ, the closed-loop system satisfies the following properties [20]: (1) the closed-loop system is internal stable, which means all the eigenvalues of the state matrix in the closed-loop system are in the left half open complex plane and (2) the H∞ norm of the closed-loop transfer function $T_{wz}(s)$ from the disturbance w to the output z is less than γ, i.e, $||T_{wz}(s)||_\infty < \gamma$. The H∞ constraint condition J is as follows:

$$J = \int_0^\infty \left(z^T z - \gamma w^T w\right) \mathrm{d}t < 0. \tag{23}$$

With equation (22), the closed-loop system from equation (20) is as follows:

$$\begin{cases} \dot{\xi} = A_{cl}\xi + B_1 w, \\ z = C_1 \xi, \end{cases} \tag{24}$$

where A_{cl} is coefficient matrix, $A_{cl} = A + B_2 K$.

Theorem 1. *For equation (24), there exist symmetric positive definite matrices X and matrices S, Y. If the matrix Π satisfies*

$$\Pi = \begin{bmatrix} \mathrm{he}\left(\mathrm{AS} + B_2 Y\right) & B_1 & L & S^T C_1^T \\ * & -\gamma^2 I & -\lambda\left(B_1\right)^T & 0 \\ * & * & \lambda \mathrm{he}(S) & 0 \\ * & * & * & -I \end{bmatrix} < 0, \tag{25}$$

$$X > 0, \tag{26}$$

where $K = YS^{-1}$, $L = X - S - \lambda(AS + B_2 Y)^T$, the given scalars are $\gamma > 0$, $\lambda < 0$, and he is the equation $he(X) = X + X^T$, and the closed-loop system of equation (24) is asymptotically stable and satisfies the H∞ constraint condition of equation (23).

Proof. The Lyapunov function is constructed as follows:

$$V(\xi) = \xi^T P \xi \geq 0, \tag{27}$$

where P is a symmetric positive definite matrix.

For the constant matrix $T_j (j = 1, 2)$ with appropriate dimension, it can be obtained from equation (23) as follows [21]:

$$\left(\xi^T T_1^T + \dot{\xi}^T T_2^T\right)\left(\dot{\xi} - A_{cl}\xi - B_1 w\right) = 0. \tag{28}$$

With equation (20), the derivation of the Lyapunov function in equation (27) is as follows:

$$\begin{aligned} \dot{V}(\xi) &= \dot{\xi}^T P \xi + \xi^T P \dot{\xi} + 2\left(\xi^T T_1^T + \dot{\xi}^T T_2^T\right)\left(\dot{\xi} - A_{cl}\xi - B_1 w\right) \\ &= \begin{bmatrix} \xi \\ w \\ \dot{\xi} \end{bmatrix}^T \begin{bmatrix} -he\left(T_1^T A_{cl}\right) & -T_1^T B_1 & J \\ * & 0 & -\left(T_2^T B_1\right)^T \\ * & * & he\left(T_2\right) \end{bmatrix} \begin{bmatrix} \xi \\ w \\ \dot{\xi} \end{bmatrix}, \end{aligned} \tag{29}$$

where $J = P + T_1{}^{\mathrm{T}} - (T_2{}^{\mathrm{T}} A_{cl})^{\mathrm{T}}$.

With equation (27), equation (23) is as follows:

$$\begin{aligned} J &= \int_0^\infty \left(z^T z - \gamma w^T w + \dot{V}\right) \mathrm{d}t - V < 0 \\ &= \int_0^\infty \left(\eta^T \Lambda \eta\right) dt - V < 0, \end{aligned} \tag{30}$$

where $\eta^{\mathrm{T}} = [\xi^{\mathrm{T}}\, w^{\mathrm{T}}\, \dot{\xi}^{\mathrm{T}}]^{\mathrm{T}}$, and

$$\Lambda = \begin{bmatrix} C_{\mathrm{cl}}^T \\ 0 \\ 0 \end{bmatrix} \begin{bmatrix} C_{\mathrm{cl}} & 0 & 0 \end{bmatrix} + \begin{bmatrix} -\mathrm{he}\left(T_1^T A_{cl}\right) & -T_1^T B_1 & J \\ * & -\gamma^2 I & -\left(T_2^T B_1\right)^T \\ * & * & he\left(T_2\right) \end{bmatrix}, \tag{31}$$

where I is the unit matrix.

Since $V(x) > 0$, equation (30) is true when $\Lambda < 0$. According to Schur lemma [20], $\Lambda < 0$ can be equivalent to the matrix, i.e.,

$$\Phi = \begin{bmatrix} -\mathrm{he}\left(T_1^T A_{cl}\right) & -T_1^T B_1 & J & C_1^T \\ * & -\gamma I^2 & -\left(T_2^T B_1\right)^T & 0 \\ * & * & \mathrm{he}\left(T_2\right) & 0 \\ * & * & * & -I \end{bmatrix} < 0. \tag{32}$$

In fact, $\Phi < 0$ can satisfy the bounded real lemma [21]. That is,

$$\begin{bmatrix} \mathrm{he}\left(\mathrm{PA}_{\mathrm{cl}}\right) & PB_1 & C_1^T \\ * & -\gamma^2 I & 0 \\ * & * & -I \end{bmatrix} < 0. \tag{33}$$

The matrix is selected such that $\Xi = \begin{bmatrix} I & 0 & 0 & 0 \\ 0 & I & 0 & 0 \\ A_{\mathrm{cl}} & B_1 & I & 0 \\ 0 & 0 & 0 & I \end{bmatrix}$, and it follows

$$\Xi^T \Phi \Xi = \begin{bmatrix} \mathrm{he}\left(\mathrm{PA}_{\mathrm{cl}}\right) & \mathrm{PB}_1 & Q & C_1^T \\ * & -\gamma^2 I & B_1^T T_2 & 0 \\ * & * & \mathrm{he}\left(T_2\right) & 0 \\ * & * & * & -I \end{bmatrix}. \tag{34}$$

So, $\Xi^T \Phi \Xi < 0$ is equivalent to $\Phi < 0$. In fact, it can be seen that equation (33) is a submatrix of equation (34). Obviously, if $\Xi^T \Phi \Xi < 0$ has a feasible solution, this solution must be the feasible solution of equation (33). So, equation (34) can satisfy the bounded real lemma.

In order to satisfy the Inequality 31, T_2 is selected a negative definite matrix, $T = -T_1$, and $\lambda T = T_2 < 0$. Inequality 31 is as follows:

$$\Psi = \begin{bmatrix} \mathrm{he}\left(T^T A_{\mathrm{cl}}\right) & T^T B_1 & P - T^T - \lambda\left(T^T A_{cl}\right)^T & C_1^T \\ * & -\gamma^2 I & -\lambda\left(T^T B_1\right)^T & 0 \\ * & * & \lambda \mathrm{he}(T) & 0 \\ * & * & * & -I \end{bmatrix} < 0. \tag{35}$$

With $A_{cl} = A + B_2 K$, equation (35) is as follows:

$$\Psi = \begin{bmatrix} \mathrm{he}\left(T^T(A+B_2K)\right) & T^TB_1 & D & C_1^T \\ * & -\gamma^2 I & -\lambda\left(T^TB_1\right)^T & 0 \\ * & * & \lambda\mathrm{he}(T) & 0 \\ * & * & * & -I \end{bmatrix} < 0, \tag{36}$$

where $D = P - T^T - \lambda(T^T(A+B_2K))^T$.

The variables are selected such that $S = T^{-1}$, $\Theta = \begin{bmatrix} S & & & \\ & I & & \\ & & S & \\ & & & I \end{bmatrix}$, and it follows

$$\begin{aligned} \Pi &= \Theta^T\Psi\Theta \\ &= \begin{bmatrix} \mathrm{he}(\mathrm{AS}+B_2\mathrm{KS}) & B_1 & E & S^TC_1^T \\ * & -\gamma^2 I & -\lambda B_1^T & 0 \\ * & * & \lambda\mathrm{he}(S) & 0 \\ * & * & * & -I \end{bmatrix} < 0, \end{aligned} \tag{37}$$

where $E = S^TPS - S - \lambda(\mathrm{AS}+B_2\mathrm{KS})^T$.

When the variables are selected, $Y = KS$ and $X = \mathrm{S}^T\mathrm{PS}$, Inequality 36 is as follows:

$$\Pi = \begin{bmatrix} \mathrm{he}(\mathrm{AS}+B_2Y) & B_1 & L & S^TC_1^T \\ * & -\gamma^2 I & -\lambda B_1^T & 0 \\ * & * & \lambda\mathrm{he}(S) & 0 \\ * & * & * & -I \end{bmatrix} < 0. \tag{38}$$

Inequality 37 is equal to equation (25). For the LPV system of equation (20), the Lyapunov stability condition of the SF H∞ system is equation (25). The proof is over. □

5. Simulation Analysis

A small USV is used as the analysis object with the parameters [22] $m_{11} = 1.956$, $m_{22} = 2.405$, $m_{33} = 0.043$, $d_{11} = 2.436$, $d_{22} = 12.992$, and $d_{33} = 0.0564$. The external disturbance is $\tau_{uw} = \tau_{rw} = \mathrm{rand}()$. Figure 2 is the control block diagram of the USV. The LOS law consists of equations (10) and (12) to produce the reference ψ_r and u_r, respectively. Equation (22) is the SF H∞ controller to produce τ_u and τ_r. The parameter K of the SF H∞ controller in equation (22) can be obtained by the LMI toolbox for the solution of Inequality 25 and Inequality 26.

To keep smooth sailing for the USV, the reference surge velocity u_r should be limited as follows:

$$u_r = \begin{cases} 3, & u_r > \dfrac{3m}{s}, \\ u_r, & 0.75U_d \le u_r \le \dfrac{3m}{s}, \\ 0.75U_d, & u_r < 0.75U_d. \end{cases} \tag{39}$$

The variable d_e is the trajectory error defined as $d_e = ((x_d)^2 + (y_d)^2)^{0.5} - (x^2 + y^2)^{0.5}$. In order to verify the SF H∞ control system performance, the ESO method [6] was used to control trajectory tracking for the USV by replacing with equation (22).

5.1. Circular Trajectory Tracking. The given reference trajectory is a circle with the function of $x_d(t) = 10\sin(0.1t)$ and $y_d(t) = 10\cos(0.1t)$. The reference trajectory is a circle with the radius of 10m, the reference speed of 1 m/s, and the initial reference input $(x_d(0), y_d(0)) = (0, 10)$. The initial position and heading angle of the USV are $x(0) = 0$ m, $y(0) = 1.5$ m, and $\psi(0) = 0$ rad; the initial velocities of the USV are set as $u(0) = 0$ m/s and $r(0) = 0$ rad/s. To demonstrate the suppression of sway velocity by the SF H∞ method, the sway velocity v is 0.2 m/s, 0.5 m/s, and 1.0 m/s for simulations.

Figure 3 shows the circular trajectory tracking with $v = 0.5$ m/s. The two curves are the trajectories by the SF H∞ control method and the ESO method, respectively. The SF method has not overshoots and can track circular trajectories more smoothly. Moreover, it has a smaller tracking error than the ESO method in the steady state.

Figures 4–6 are circular trajectory response of d_e, u, and ψ_e with different values of v. When $v = 0.2$ m/s, 0.5 m/s, and 1.0 m/s, the errors d_e of the SF H∞ method have no overshoots but those of the ESO method have overshoots of 3.4%, 7.1%, and 9.9%, as shown in Figure 4. System response of the surge velocity u by the SF H∞ method has overshoots of 3.4%, 7.1%, and 9.9% but those by the ESO method have overshoots of 17.4%, 18.9%, and 28.8%, as shown in Figure 5. In Figure 6, system response ψ_e by the SF H∞ method has overshoots of 16.2%, 24.2%, and 30.3% but those by the ESO method have 56.1%, 64.4%, and 83.3%, respectively. Moreover, the steady-state error between the surge velocity u and the reference u_r increases when v increases, but the error increment by the SF H∞ method is smaller than the ESO method, as shown in Figure 5. So, whatever the value of v, thr SF H∞ method has the better performance on dynamic and stable indices than those by the ESO method in circular trajectory.

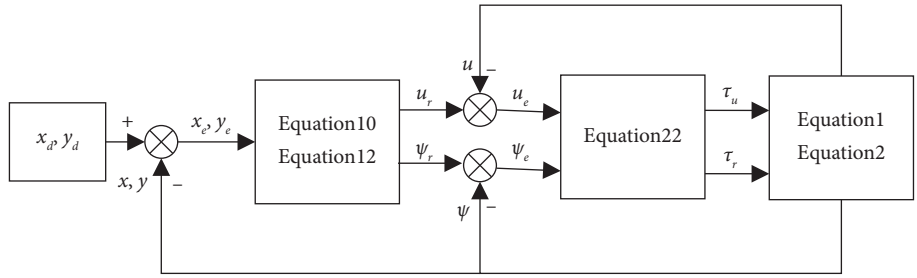

Figure 2: Control block diagram.

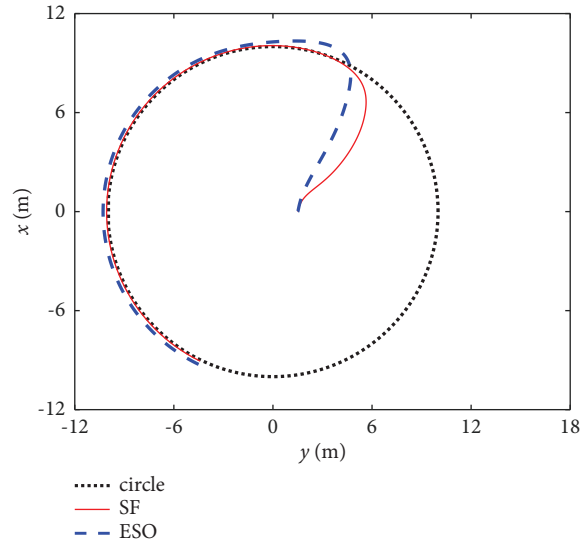

Figure 3: Circular trajectory.

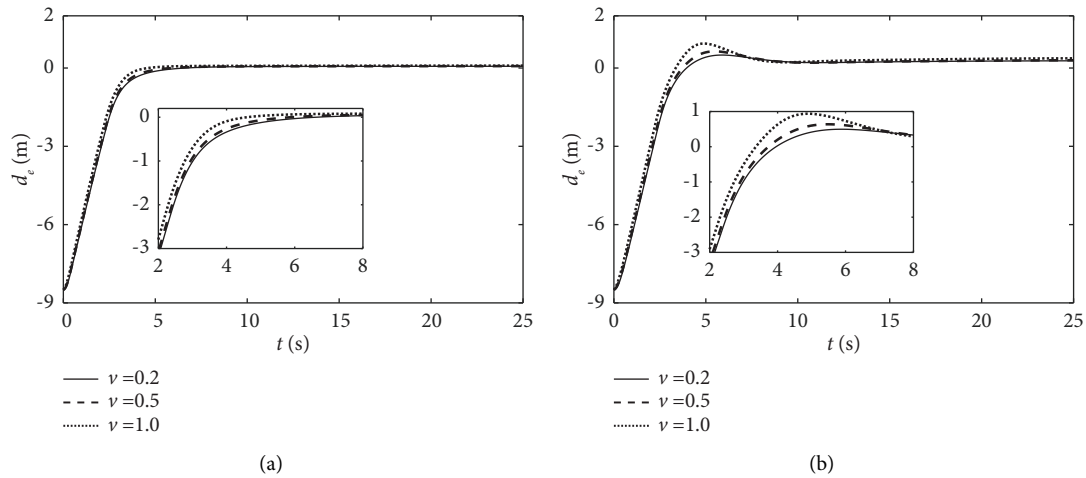

Figure 4: Circular trajectory error d_e with v. (a) SF H∞ method. (b) ESO method.

5.2. Straight Trajectory Tracking. The reference input is a straight trajectory of $x_d = \sqrt{2}/2t$ and $y_d = \sqrt{2}/2t$ with the initial position $(x_d(0), y_d(0)) = (0, 0)$. The initial position and heading angle of the USV are set as follows: $x(0) = 0$ m, $y(0) = 1.5$ m, and $\psi(0) = 0$ rad; USV initial velocities are set as follows: $u(0) = 0$ m/s and $r(0) = 0$ rad/s. To demonstrate the suppression of the sway velocity by the SF H∞ method, v are set as $v = 0.2$ m/s, 0.5 m/s, and 1.0 m/s in simulations.

Figure 7 is straight trajectory tracking by the SF H∞ method and the ESO method with $v = 0.5$ m/s. The SF H∞ method can track straight trajectory earlier and faster than the ESO method, which is also reflected with the trajectory

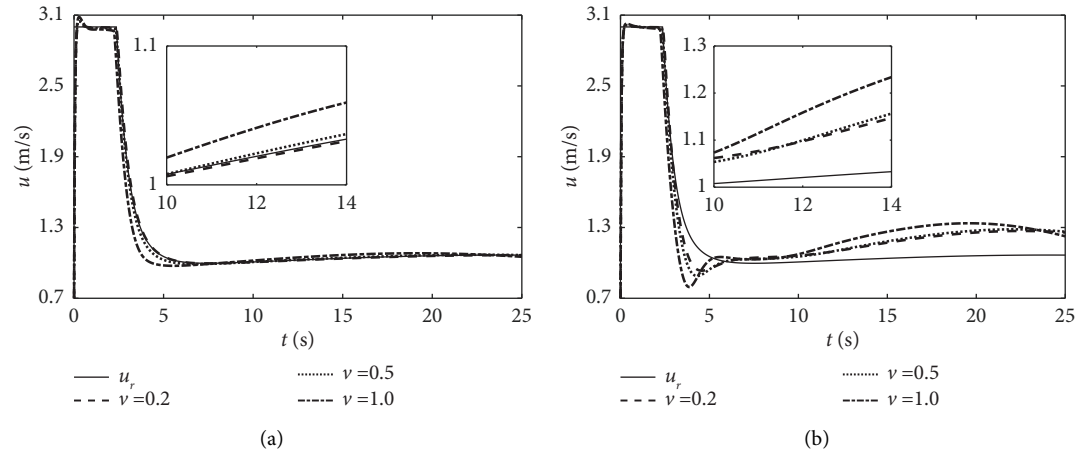

Figure 5: Circular trajectory system response u. (a) SF H∞ method. (b) ESO method.

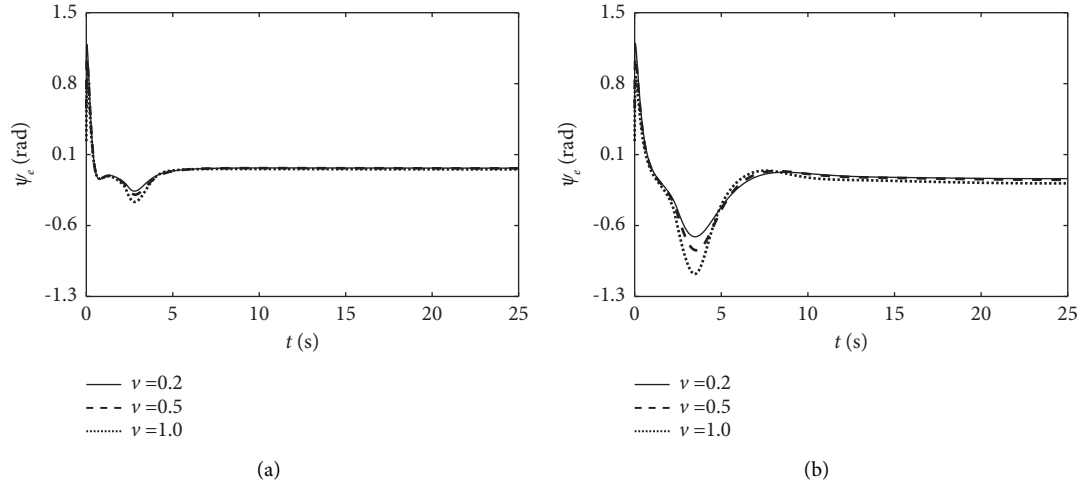

Figure 6: Circular trajectory system response ψ_e. (a) SF H∞ method. (b) ESO method.

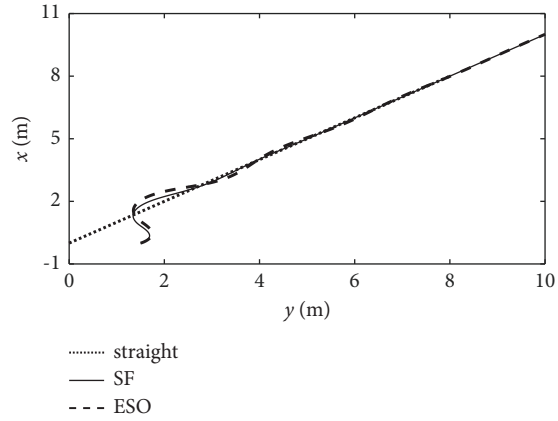

Figure 7: Straight trajectory.

error d_e in Figure 8. Moreover, d_e overshoots by the SF H∞ method are 0.0%, 5.1%, and 21.3% while for the ESO method are 3.9%, 13.5% ,and 38.7% with $v = 0.2$ m/s, 0.5 m/s, and 1.0 m/s. The overshoot d_e increases when v increases, but the corresponding overshoot by the SF H∞ method is smaller than that by the ESO method. Figures 9(a) and 10 are the system responses u and ψ. When v increases, the adjust time for u and ψ increases, especially for the ESO method. When

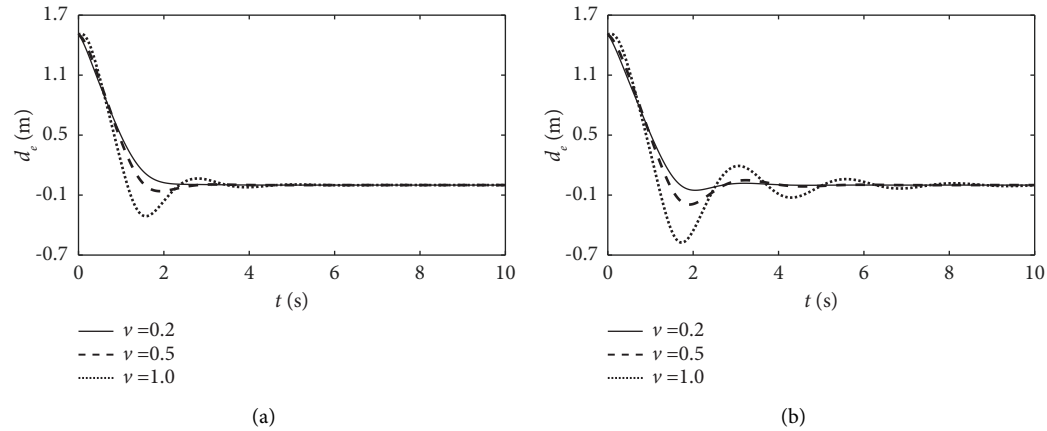

Figure 8: Straight trajectory error d_e with v. (a) SF H∞ method. (b) ESO method.

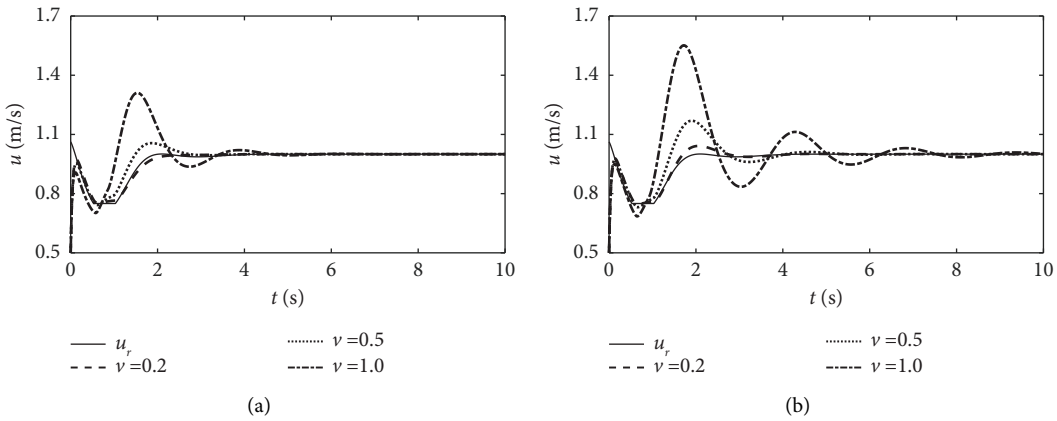

Figure 9: Straight trajectory system response u. (a) SF H∞ method. (b) ESO method.

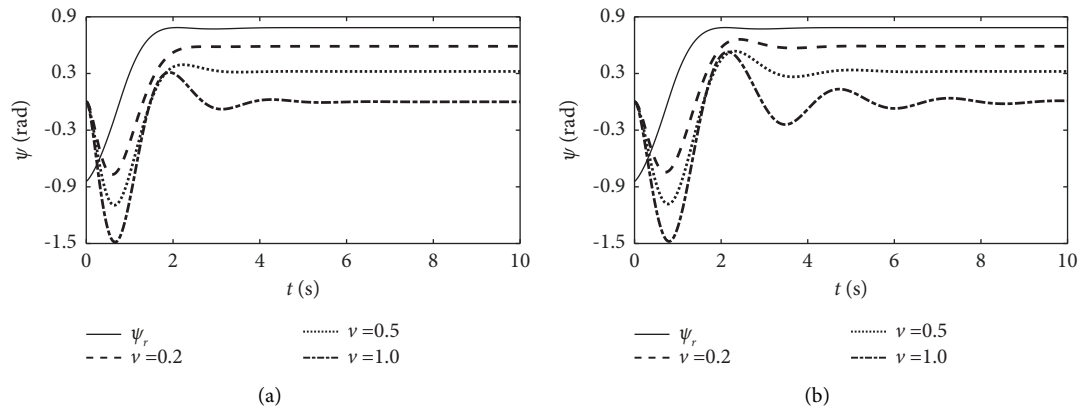

Figure 10: Straight trajectory system response ψ. (a) ψ by SF in different v. (b) ψ by ESO in different v.

$v = 0.2$ m/s, 0.5 m/s, and 1.0 m/s, the system response u by the SF H∞ method has overshoots of 0.4%, 5.8%, and 31.7% while the ESO method has overshoots of 4.1%, 17.6%, and 55.3%. The system response ψ by the SF H∞ method has overshoots of 0.0%, 3.8% and 18.2% while the ESO method has overshoots of 4.8%, 12.7% and 30.3%, respectively. Moreover, the steady-state error of ψ is larger when v increases. So, the SF H∞ method has the better performance on dynamic and stable indices than those by the ESO method for straight trajectory tracking.

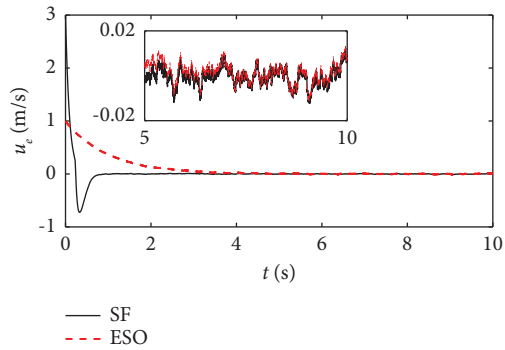

Figure 11: System error u_e.

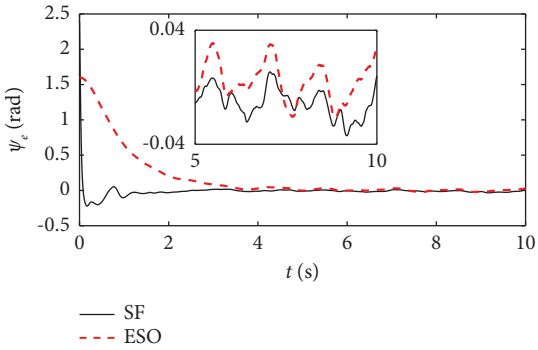

Figure 12: System error ψ_e.

5.3. Robustness Analysis. In order to analyze the system robustness, the uncertainties are imposed as $\tau_{uw} = \tau_{rw} = \kappa(\text{rand}())$ with $\kappa = 1$, 2, and 4, respectively. The larger the κ, the larger the uncertainties are. The steady-state errors u_e and ψ_e are used to evaluate the system robustness to suppress the uncertainties with the different κ. Figures 11 and 12 are the steady-state errors u_e and ψ_e with $\kappa = 2$. When $\kappa = 1$, 2, and 4, the ranges of the steady-state error u_e are ±0.008 m/s, ±0.012 m/s, and ±0.015 m/s by the SF H∞ method and ±0.012 m/s, ±0.016 m/s, and ±0.022 m/s by the ESO method. The ranges of the steady-state error ψ_e are ±0.021 rad, ±0.032 rad, and ±0.044 rad by the SF H∞ method and ±0.028 rad, ±0.037 rad, and ±0.051 rad by the ESO method. Moreover, the steady-state errors u_e and ψ_e of the SF H∞ control system have smaller increment than the ESO system, which indicates the SF H∞ control system has the stronger robustness than the ESO system.

6. Conclusions

With consideration of the sway velocity and the uncertainties and the disturbance of wind, wave, and currentW the SF H∞ control method is proposed for trajectory tracking of the USV to improve the system performance. First, the position error mode of trajectory tracking is established to design the LOS law to produce the reference heading angle and surge velocity. Second, the LPV system with sway velocity is established to design the SF H∞ controller for the heading angle and the surge velocity. The Lyapunov function is constructed to obtain the asymptotical stability for the LPV since the asymptotical stability has coupling terms of the variable parameter v and can be directly solved by the novel variable replacement method. Moreover, the parameters of the SF H∞ controller are obtained by the LMI tool. Finally, the simulation results show that (1) the LOS guidance law can produce the reference heading angle and the reference surge velocity for trajectory tracking and (2) the SF H∞ method has the better system performance on dynamic, steady-state indices for circular and straight trajectory tracking than the ESO method to suppress the sway velocity and also on system robustness. In this work, the proposed method does not consider the convergence of LOS.

Data Availability

The data used to support the findings of this study are included within the supplementary file.

Conflicts of Interest

The authors declare that there are no conflicts of interest regarding the publication of this paper.

Acknowledgments

This research was funded by the Natural Science Foundation of Fujian under project 2019H0007, Fujian Young and Middle-Aged Teachers Science and Technology Research Project JAT220564.

References

[1] R. Chu, Z. Liu, and Z. Chu, "Improved super-twisting sliding mode control for ship heading with sideslip angle compensation," *Ocean Engineering*, vol. 260, Article ID 111996, 2022.

[2] Y. Huang, X. Zou, C. Xie, and Y. Zhang, "Ultrahigh extinction ratio and ultralow insertion loss for polarization beam splitter based on two folded asymmetrical directional couplers with dual-stage etching," *Applied Optics*, vol. 62, no. 4, pp. 965–971, 2023.

[3] C. Xiao, L. Zhong, and Z. Jianqiang, "Adaptive sliding-mode path following control system of the underactuated USV under the influence of ocean currents," *Journal of Systems Engineering and Electronics*, vol. 29, no. 6, pp. 1271–1283, 2018.

[4] L. Wan, Y. Su, H. Zhang, B. Shi, and M. S. AbouOmar, "An improved integral light-of-sight guidance law for path following of unmanned surface vehicles," *Ocean Engineering*, vol. 205, Article ID 107302, 2020.

[5] Y. Su, L. Wan, D. Zhang, and F. Huang, "An improved adaptive integral line-of-sight guidance law for unmanned surface vehicles with uncertainties," *Applied Ocean Research*, vol. 108, Article ID 102488, 2021.

[6] H. Huang, M. Gong, Y. Zhuang, S. Sharma, and D. Xu, "A new guidance law for trajectory tracking of an underactuated unmanned surface vehicle with parameter perturbations," *Ocean Engineering*, vol. 175, pp. 217–222, 2019.

[7] C. Lv, H. Yu, N. Zhao, J. Chi, H. Liu, and L. Li, "Robust state-error port-controlled Hamiltonian trajectory tracking control

for unmanned surface vehicle with disturbance uncertainties," *Asian Journal of Control*, vol. 24, no. 1, pp. 320–332, 2022.

[8] R. Miao, Z. Dong, L. Wan, and J. Zeng, "Heading control system design for a micro-USV based on an adaptive expert S-PID algorithm," *Polish Maritime Research*, vol. 25, no. 2, pp. 6–13, 2018.

[9] J. Zhang, S. Yu, D. Wu, and Y. Yan, "Nonsingular fixedtime terminal sliding mode trajectory tracking control for marine surface vessels with anti-disturbances," *Ocean Engineering*, vol. 217, Article ID 108158, 2020.

[10] M. Fu, M. Li, and W. Xie, "Finite-time trajectory tracking fault-tolerant control for surface vessel based on time-varying sliding mode," *IEEE Access*, vol. 6, pp. 2425–2433, 2018.

[11] J. Dong, M. Zhao, M. Cheng, and Y. Wang, "Integral terminal sliding-mode integral backstepping adaptive control for trajectory tracking of unmanned surface vehicle," *Cyber-Physical Systems*, vol. 9, no. 1, pp. 77–96, 2023.

[12] D. Mu, G. Wang, Y. Fan, B. Qiu, and X. Sun, "Adaptive course control based on trajectory linearization control for unmanned surface vehicle with unmodeled dynamics and input saturation," *Neurocomputing*, vol. 330, pp. 1–10, 2019.

[13] J. Y. Juang and B. Chang, "Robust control theory applied to ship maneuvering," in *Proceedings of the 38th IEEE Conference on Decision and Control*, pp. 2186–2191, New York, NY, USA, December 1999.

[14] J. Xiong, Y. He, and J. Han, "Robust heading control of an unmanned surface vehicle based on LPV model," *Journal of System Simulation*, vol. 32, no. 8, pp. 1598–1605, 2020.

[15] J. Xiong, D. Li, and Y. He, "Robust H∞ yaw tracking control of a water-jet propulsion unmanned surface vehicle," *Control Theory & Applications*, vol. 36, pp. 165–174, 2019.

[16] Y. Huang, Z. Liu, W. Huang, and S. Chen, "Robust H∞ control for nonlinear course system of unmanned surface vessel with polytopic uncertainty based on sum of squares," *Transactions of the Institute of Measurement and Control*, vol. 43, no. 2, pp. 390–399, 2021.

[17] Z. X. Liu, C. Yuan, and Y. M. Zhang, "Linear parameter varying adaptive control of an unmanned surface vehicle," *IFAC-PapersOnLine*, vol. 48, no. 16, pp. 140–145, 2015.

[18] Y. Huang, X. Shi, W. Huang, and S. Chen, "Internal model control-based observer for the sideslip angle of an unmanned surface vehicle," *Journal of Marine Science and Engineering*, vol. 10, no. 4, p. 470, 2022.

[19] Y. Huang, T. Lin, and W. Huang, "Extended bounded real lemma-based sum of squares for static output feedback H∞ heading control," *International Journal of Robust and Nonlinear Control*, vol. 32, no. 14, pp. 7879–7895, 2022.

[20] Y. He, M. Wu, and J. H. She, "Improved bounded-real-lemma representation and H∞ control of systems with polytopic uncertainties," *IEEE Transactions on Circuits and Systems II: Express Briefs IEEE*, vol. 52, no. 7, pp. 380–383, 2005.

[21] S. Marir, M. Chadli, and M. V. Basin, "Bounded real lemma for singular linear continuous-time fractional-order systems," *Automatica*, vol. 135, Article ID 109962, 2022.

[22] R. Yu, Q. Zhu, G. Xia, and Z. Liu, "Sliding mode tracking control of an underactuated surface vessel," *IET Control Theory & Applications*, vol. 6, no. 3, pp. 461–466, 2012.